EUROPEAN ORGANIZATION FOR NUCLEAR RESEARCH

CERN-EP/98-206
17 December 1998

Study of Neutral–Current Four–Fermion and ZZ Production in e^+e^- Collisions at $\sqrt{s} = 183$ GeV

L3 Collaboration

Abstract

A study of neutral–current four–fermion processes is performed using a data sample corresponding to 55.3 pb^{-1} of integrated luminosity collected by the L3 detector at LEP at an average centre–of–mass energy of 183 GeV. The neutral–current four–fermion cross sections for final states with a pair of charged leptons plus jets and with four charged leptons are measured to be consistent with the Standard Model predictions.

Events with fermion pair masses close to the Z boson mass are selected in all observable final states and the ZZ production cross section is measured to be $\sigma_{\mathrm{ZZ}} = 0.30^{+0.22}_{-0.16}\,^{+0.07}_{-0.03}$ pb, in agreement with the Standard Model expectation. No evidence for the existence of anomalous triple gauge boson ZZZ and ZZγ couplings is found and limits on these couplings are set.

To be submitted to Physics Letters B

1 Introduction

Neutral current four–fermion final states are an important class of events to be studied at LEP for two main reasons. Firstly, the study of these events carries new experimental information about the structure of electroweak interactions [1, 2], thus allowing new tests of Standard Model (SM) predictions in e^+e^- collisions at energies never attained before. Secondly, measurements of their production rates and distributions differing from the expectations of the SM could signal the existence of new physics.

In this paper we describe a study of four–fermion events produced via the exchange of neutral gauge bosons. They arise from several production mechanisms, as shown in Figure 1. At the centre–of–mass energy of 183 GeV the production of two on–shell Z bosons is possible. If the exchanged bosons are both Z, the contribution of the conversion diagram is dominant in the SM.

We report the results of the analysis of final states with a pair of charged leptons and jets, $\ell^+\ell^-\mathrm{q\bar{q}}$ (ℓ = e, μ, τ), and with four charged leptons, $\ell^+\ell^-\ell'^+\ell'^-$. The cross section of these processes is measured. The results of an analysis of neutral–current four–fermion events from the data collected at centre–of–mass energies of 161 GeV and 172 GeV are reported in Ref. [3].

Events with fermion pair masses close to the Z boson mass are selected in $\ell^+\ell^-\mathrm{q\bar{q}}$ and $\ell^+\ell^-\ell'^+\ell'^-$ final states, as well as in final states with two charged leptons and missing energy, $\ell^+\ell^-\nu\bar{\nu}$, with jets and missing energy, $\mathrm{q\bar{q}}\nu\bar{\nu}$, and with four jets, $\mathrm{q\bar{q}q'\bar{q}'}$. The data show evidence of on–shell ZZ production, for which the cross section is measured. The results of the ZZ analysis are interpreted in terms of anomalous ZZZ and ZZγ couplings.

2 Data and Monte Carlo Samples

The data analysed were collected by the L3 detector [4] at LEP in 1997 and correspond to an integrated luminosity of 55.3 pb^{-1} at an average centre–of–mass energy of 182.7 GeV. The actual centre–of–mass energies and luminosities are: 3.9 pb^{-1} at $\sqrt{s}$ =181.74 GeV, 49.6 pb^{-1} at $\sqrt{s}$ =182.72 GeV and 1.8 pb^{-1} at $\sqrt{s}$ =183.81 GeV.

The EXCALIBUR [5] Monte Carlo is used to simulate the neutral–current four–fermion events. Background from fermion–pair production is simulated with PYTHIA 5.72 [6] ($e^+e^- \rightarrow \mathrm{q\bar{q}}(\gamma)$), KORALZ 4.02 [7] ($e^+e^- \rightarrow \mu^+\mu^-(\gamma)$ and $e^+e^- \rightarrow \tau^+\tau^-(\gamma)$) and BHAGENE 3 [8] ($e^+e^- \rightarrow e^+e^-(\gamma)$). Background from charged–current four–fermion processes is generated with EXCALIBUR for $\mathrm{e}\nu_\mathrm{e}\mathrm{q\bar{q}}$ and $\ell^+\nu_\ell\ell^-\bar{\nu}_\ell$ and KORALW 1.21 [9] for on–shell $\mathrm{W^+W^-}$ production. Contributions from multiperipheral processes are studied using events generated with PHOJET 1.05c [10] ($e^+e^- \rightarrow e^+e^-\mathrm{q\bar{q}}$) and DIAG36 [11] ($e^+e^- \rightarrow e^+e^-\ell^+\ell^-$).

The L3 detector response is simulated using the GEANT 3.15 program [12], which takes into account the effects of energy loss, multiple scattering and showering in the detector. The GEISHA program [13] is used to simulate hadronic interactions in the detector.

3 Study of Four–Fermion Production

The four–fermion signal is defined using generated $e^+e^- \to \ell^+\ell^- q\bar{q}$ and $e^+e^- \to \ell^+\ell^-\ell'^+\ell'^-$ events requiring a minimum momentum of the outgoing fermions of 1 GeV, a minimum invariant mass of each combination of two fermions of 1 GeV and a minimum value of the polar angle θ of the outgoing fermions with respect to the beam axis of 5°. The predicted cross sections for four–fermion events are reported in Table 1.

Two different selections are developed, one for the $\ell^+\ell^- q\bar{q}$ and another for the $\ell^+\ell^-\ell'^+\ell'^-$ final states.

3.1 The $\ell^+\ell^- q\bar{q}$ Event Selection

The $\ell^+\ell^- q\bar{q}$ events are characterised by hadronic jets and a pair of leptons isolated from the hadronic system. Only configurations with a pair of isolated electrons or muons are investigated. No dedicated selection of $\tau^+\tau^- q\bar{q}$ events is performed. At least 5 tracks and 15 calorimetric clusters are required. The visible energy must be larger than $0.5\sqrt{s}$. The energy of each lepton is required to be at least 3 GeV. The background comes from hadronic events like those produced by $e^+e^- \to q\bar{q}(\gamma)$ and $e^+e^- \to W^+W^-$ processes.

The distributions of the invariant mass of the two selected leptons and their recoil mass are shown for the data and the SM expectations, in Figures 2a and 2b. The number of observed events, of expected signal and background events, as well as signal efficiencies, are reported in Table 2.

3.2 The $\ell^+\ell^-\ell'^+\ell'^-$ Event Selection

To reject high multiplicity events, we require less than 10 tracks and less than 15 calorimetric clusters in the event. The visible energy must be larger than $0.2\sqrt{s}$. At least four leptons are required in the event. If there is an energy deposition in the low polar angle calorimeters, three identified leptons suffice. At least two of the selected leptons must have the same flavour. A minimum energy of 2 GeV for electrons and 3 GeV for muons and taus is required. Background comes from lepton pair production ($e^+e^- \to \ell^+\ell^-(\gamma)$) with photon radiation.

The distributions of the highest invariant mass of the pair of leptons of the same flavour and their recoil mass are shown for the data and the SM expectations in Figures 2c and 2d. The number of observed events, of expected signal and background events, as well as signal efficiencies, are reported in Table 2.

3.3 Measurement of the Four–Fermion Cross Section

The cross sections $\sigma_{\ell^+\ell^- q\bar{q}}$ and $\sigma_{\ell^+\ell^-\ell'^+\ell'^-}$ of the $e^+e^- \to \ell^+\ell^- q\bar{q}$ and $e^+e^- \to \ell^+\ell^-\ell'^+\ell'^-$ processes are determined in a two–variable maximum–likelihood fit, as described in [3]. The fit is based on Poisson statistics and takes into account small cross efficiencies between the selections. Systematic errors on signal and background expectations are estimated by varying the selection cuts within the experimental resolutions. Further uncertainties arise from limited Monte Carlo statistics. The systematic error induced on the measured cross section by the uncertainties on signal and background predictions is determined as the standard deviation of the distribution of the cross section values obtained by varying signal and background predictions according to Gaussian distributions with standard deviations equal to their errors.

The measured cross sections are

$$\sigma_{\ell^+\ell^-\mathrm{q\bar{q}}} = 2.4^{+0.9}_{-0.7} \pm 0.1\,\mathrm{pb}, \qquad \sigma_{\ell^+\ell^-\ell'^+\ell'^-} = 1.3^{+0.8}_{-0.6} \pm 0.1\,\mathrm{pb},$$

where the first error is statistical and the second is systematic. These results agree with the SM expectations of 1.8 pb and 1.0 pb, respectively.

4 Study of On–Shell ZZ Production

The on–shell ZZ signal is defined by phase–space cuts at generator level requiring that the masses of the generated fermion pairs in the final state, $\mathrm{M_{f\bar{f}}}$ and $\mathrm{M_{f'\bar{f}'}}$, be in the range between 70 GeV and 105 GeV. In the final states with electrons, these are required to be in the polar angular range $|\cos\theta_\mathrm{e}| < 0.95$. In final states with four fermions of the same flavour, for at least one of the two possible fermion pair combinations, the fermion pair masses must be in the range mentioned above. In the final states $\mathrm{u\bar{u}d\bar{d}}$, $\mathrm{c\bar{c}s\bar{s}}$ and $\nu_\ell\bar{\nu}_\ell\ell^+\ell^-$ ($\ell = \mathrm{e}, \mu, \tau$), there is a large contribution from W exchange. To reduce this contribution we require that the masses of the fermion pairs susceptible to come from a W decay be either smaller than 75 GeV or larger than 85 GeV. The distributions of the masses generated by the EXCALIBUR Monte Carlo at $\sqrt{s}$=182.72 GeV for $\mathrm{e^+e^-} \rightarrow \mathrm{q\bar{q}q'\bar{q}'}$ and $\mathrm{e^+e^-} \rightarrow \ell^+\ell^-\mathrm{q\bar{q}}$ events before and after the generator level cuts described above are shown in Figure 3.

The total expected ZZ cross section is 0.25 pb at $\sqrt{s}$ =182.72 GeV. Contributions from different final states are reported in Table 3. In some cases there are relevant contributions from processes other than the on-shell ZZ production. Low–mass fermion pairs are abundantly produced by photon mediated conversion and annihilation processes in which, in case of final states with fermion pairs of the same flavour, one combination can satisfy our mass requirements. Final states with electrons or electron neutrinos have large contributions from multiperipheral and charged–current exchange processes.

The ZZ cross section rises steeply in the centre–of–mass energy range investigated and amounts to 0.19 pb and 0.32 pb at $\sqrt{s}$ =181.74 GeV and 183.81 GeV, respectively. However, the luminosity weighted average of the expected cross section is not altered from the value given above and the uncertainty of the LEP beam energy of 25 MeV [14] does not lead to a sizeable error on it.

Different event selections, for $\ell^+\ell^-\mathrm{q\bar{q}}$, $\ell^+\ell^-\ell'^+\ell'^-$, $\ell^+\ell^-\nu\bar{\nu}$, $\mathrm{q\bar{q}}\nu\bar{\nu}$ and $\mathrm{q\bar{q}q'\bar{q}'}$ final states are optimised for events with high mass fermion pairs.

4.1 The $e^+e^- \rightarrow ZZ \rightarrow \ell^+\ell^- q\bar{q}$ Event Selection

Selections for each final state with electrons, muons and taus are performed. Events are accepted if they pass at least one of the selections.

A common preselection is applied requiring high multiplicity events with more than 9 tracks and more than 15 calorimetric clusters. The visible energy must be larger than $0.8\sqrt{s}$, $0.7\sqrt{s}$ and $0.4\sqrt{s}$ for events with electron, muon and tau pairs, respectively. The electron energy is required to be in the range between 20 GeV and 60 GeV whereas the muon energy must be larger than 20 GeV for muons identified in the muon spectrometer and larger than 6 GeV for muons identified by their characteristic signature of a minimum ionising particle. The opening angle between the two electrons or muons and the two jets has to exceed 120°. The $e^+e^-q\bar{q}$ and $\mu^+\mu^-q\bar{q}$ events are subject to the DURHAM algorithm [15] with $\log(Y_{34}) \geq -6$, Y_{34} being the value of the jet resolution parameter for which the event goes from a four–jet to a three–jet topology. For the $e^+e^-q\bar{q}$ channel we require in addition the invariant mass of the two electrons to be larger than 70 GeV and the ratio of the missing transverse momentum to the visible energy to be less than 0.1.

Two independent analyses are performed for the $\tau^+\tau^-q\bar{q}$ events: a selection based on tau identification and a jet based selection. An event is accepted if it satisfies either of the two selections. In the first selection, tau leptons are identified via their decay into isolated electrons or muons, or as an isolated low–multiplicity jet with 1 or 3 tracks and unit charge. The visible energy must be less than $0.95\sqrt{\mathrm{s}}$ and the missing momentum parallel to the beam axis smaller than 30 GeV. In the jet based selection, the event is forced into four jets using the DURHAM algorithm. Two of the jets must have less than 4 tracks. These jets are then considered as τ candidates. The visible mass must be less than $0.87\sqrt{\mathrm{s}}$, the ratio between missing and visible energy be less than 0.25 and the ratio between the missing momentum parallel and transverse to the beam axis be less than 3. In both selections, the opening angle between the two τ candidates and between the two jets must be larger than 130°. Their invariant masses must be within 70 GeV and 120 GeV. The invariant masses of the tau pair and of the jet pair are calculated from a kinematic fit twice, once imposing four–momentum conservation and a second time imposing in addition that the masses be equal. The ratios of the masses resulting from the two fits are required to be between 0.8 and 1.2.

The results for the $\ell^+\ell^-q\bar{q}$ event selections are summarised in Table 4. The background is dominated by $W^+W^- \rightarrow \ell\nu q\bar{q}$ events (55%). The remaining background consists of $e^+e^- \rightarrow q\bar{q}(\gamma)$ (22%) and neutral–current four–fermion events (23%) outside the ZZ signal definition cuts. The errors on signal and background predictions are dominated by uncertainties in the energy scale, the lepton identification and isolation. An error of 15% on the expected number of background events and 4% on the signal efficiency is assigned.

One of the two selected events in the data is shown in Figure 4. The spectrum of the mass obtained from a kinematic fit, imposing four–momentum conservation and equal masses of the lepton and the jet pair, M_{5C}, is shown in Figure 5.

4.2 The $e^+e^- \rightarrow ZZ \rightarrow \ell^+\ell^-\ell'^+\ell'^-$ Event Selection

The $ZZ\rightarrow \ell^+\ell^-\ell'^+\ell'^-$ selection is developed for all charged leptonic final states other than $\tau^+\tau^-\tau^+\tau^-$ events. At least four leptons are required in the event. The electrons must have an energy of at least 15 GeV, relaxed to 3 GeV for other leptons. The invariant masses of the combinations of two same flavour leptons are then calculated and the lepton pair whose mass is the closest to the Z boson mass is chosen. This mass and the recoil mass to the chosen lepton pair are required to be in the range between 70 GeV and 105 GeV. The distribution of the average of the two masses, M_{av}, is shown in Figure 6a.

The main background in this selection is constituted by lepton pair production and neutral–current four–fermion events outside the ZZ signal definition cuts. The signal efficiency depends on the final state, ranging from 15% for $e^+e^-\tau^+\tau^-$ events up to 78% for $e^+e^-\mu^+\mu^-$ events. The signal efficiency, the expected signal and background and the observed events are reported in Table 4. The errors on the expected signal and background events are due to the lepton identification and the limited Monte Carlo statistics, the latter giving the dominant contribution to the error on the background expectation. Errors of 25% and 10% are assigned to the expected number of background and signal events, respectively.

4.3 The $e^+e^- \rightarrow ZZ \rightarrow \ell^+\ell^-\nu\bar{\nu}$ Event Selection

The $\ell^+\ell^-\nu\bar{\nu}$ events, with ℓ either a muon or an electron, are selected requiring two same flavour leptons. These event are required to have less than 3 tracks, less than 6 calorimetric clusters and a visible energy in the range between 80 GeV and 100 GeV. In order to remove the background from lepton pair production we select only events with $|\cos\theta_{miss}| < 0.7$ and $129^\circ < \alpha < 178^\circ$, where θ_{miss} is the polar angle of the missing momentum and α the angle between the leptons. The contribution from cosmic rays is suppressed requiring at least one scintillator in time in events with muon pairs. The lepton pair mass, M_{vis}, must be in the range 70 GeV to 105 GeV and the mass recoiling against the leptons, M_{rec}, in the range 70 GeV to 100 GeV. The dominant background is given by four–fermion events outside the ZZ signal definition cuts.

The sum of the visible and recoil masses, $M_{vis} + M_{rec}$, for the data and the expected background and signal is shown in Figure 6b. The signal efficiency is 37% for electron and 33% for muon events. The expected signal, background and the observed events are reported in Table 4. The errors on the expected signal and background events are due to the lepton identification and the limited Monte Carlo statistics. They are evaluated to be at most 10% for both signal and background.

4.4 The $e^+e^- \rightarrow ZZ \rightarrow q\bar{q}\nu\bar{\nu}$ Event Selection

High multiplicity hadronic events with at least four charged tracks are selected with energy deposition in the electromagnetic calorimeter larger than 10 GeV. All calorimetric clusters in the event are combined to form two hadronic jets using the DURHAM algorithm. The invariant mass of the two jets, M_{vis}, must be in the range 60 GeV to 125 GeV. The energy in the low polar angle calorimeters is required to be smaller than 10 GeV. These cuts reduce contributions from the purely leptonic final states $e^+e^- \to \ell^+\ell^-(\gamma)$ and multiperipheral interactions $e^+e^- \to e^+e^-f\bar{f}$. The $e^+e^- \to q\bar{q}(\gamma)$ events are rejected requiring the transverse missing energy to exceed 5 GeV and the longitudinal momentum not to exceed 40% of the visible energy. The missing momentum vector must point at least 17° away from the beam axis and the energy in the 25° azimuthal sector around its direction must be below 20 GeV.

In order to reduce the remaining background from $e^+e^- \to W^+W^-$ production where one of the W bosons decays into leptons, events containing identified leptons with energy greater than 20 GeV are rejected. In addition, the solid angle defined by the directions of the three jets, formed using the DURHAM algorithm, must be smaller than 5.5 steradians. The value of the jet resolution parameter of the JADE algorithm [16] for which the number of jets in the event changes from three to two must be smaller than 0.06, and the value for which the number of jets changes from four to three must be smaller than 0.02.

To further differentiate between the signal and the WW background, the discriminant variable NN is constructed using a neural network approach [17]. The inputs to the neural network include event shape variables, the event mass, the masses of the two jets and the total missing momentum. The signal events populate preferentially the region of high NN values. A lower cut on the NN variable is applied to maximise the signal to background ratio.

The signal efficiency, the expected signal and background and the observed events are reported in Table 4. The errors on signal and background expectations are mainly determined by the uncertainty on the energy calibration and the limited Monte Carlo statistics: they are 4% and 5% for signal and background, respectively. The sum of the visible and recoil masses, $M_{vis} + M_{rec}$, for the data and the expected background and signal is shown in Figure 6c. The signal events populate predominantly the region from 175 GeV to 183 GeV.

4.5 The $e^+e^- \to ZZ \to q\bar{q}q'\bar{q}'$ Event Selection

The $q\bar{q}q'\bar{q}'$ events are selected and reconstructed into four jets as described in [18]. A kinematic fit imposing four–momentum conservation is applied to the four jets to improve the di–jet mass resolution. The four jets are paired into two di–jets, each of which is required to have more than four tracks, to suppress the contamination from $\tau^+\tau^-q\bar{q}$ events. Of the three possible pairing combinations, the one with minimum mass χ^2 to the assumption of a Z pair is chosen. The ZZ candidates are selected if $M_{5C} > 85$ GeV.

The expected signal, background and observed data events after selection are reported in Table 4. The errors on signal and background expectations are mainly determined by the uncertainty on the energy calibration and the limited Monte Carlo statistics: they are 6% and 4% for signal and background, respectively.

A neural network method [17] is used to distinguish the $e^+e^- \to ZZ \to q\bar{q}q'\bar{q}'$ events from the $e^+e^- \to q\bar{q}(\gamma)$ and $e^+e^- \to W^+W^-$ backgrounds. The input variables include the event thrust, the ratio of the transverse energy to the total energy, the Y_{34} value, the ratios of the minimum to the maximum jet energies, the minimum and maximum opening angles between jets, the di-jet masses and the χ^2 values of equal mass fits for $\mathrm{W^+W^-}$ or ZZ pairs hypothesis. The three neural network outputs for $\mathrm{e^+e^-} \rightarrow \mathrm{q\bar{q}}(\gamma)$, $\mathrm{W^+W^-}$ and ZZ events, denoted as $\mathrm{NN_{qq}}$, $\mathrm{NN_{WW}}$ and $\mathrm{NN_{ZZ}}$, respectively, and $\mathrm{M_{5C}}$ are combined into the variable $\xi = \mathrm{NN_{ZZ}}(1 - \mathrm{NN_{qq}})(1 - \mathrm{NN_{WW}})(2\mathrm{M_{5C}}/\sqrt{\mathrm{s}})$. The ξ distribution for the data, the background and the ZZ signal is shown in Figure 6d.

4.6 Measurement of the ZZ Cross Section

A binned Poissonian log–likelihood fit to the spectra of Figures 5 and 6 is used to combine the results described above. In this fit the ratio of the measured cross section to the SM value as predicted by EXCALIBUR is determined from the maximum of the likelihood. The measured cross section is

$$\sigma_{\mathrm{ZZ}} = 0.30^{+0.22}_{-0.16}\,{}^{+0.07}_{-0.03}\,\mathrm{pb}.$$

The systematic error is estimated taking into account the errors on signal and background expectations, given in Table 4, using a method similar to the one described in Section 3.3. This measured cross section value is in good agreement with the SM. At 95% confidence level one obtains $0.03 < \sigma_{\mathrm{ZZ}} < 0.79\,\mathrm{pb}$, where the statistical and systematic errors have been combined in quadrature. Figure 7 shows separately the likelihoods of the most significant analyses and the combined one as a function of the ratio of the measured to the SM cross section.

5 Limits on Anomalous Couplings

The most general Lorentz invariant expressions including anomalous couplings are given in Ref. [19]. Deviations from the SM are described by means of four anomalous couplings $\mathrm{f_i^V}$ ($\mathrm{i} = 4, 5; \mathrm{V} = \gamma, \mathrm{Z}$), where the V superscript corresponds to an anomalous coupling ZZV. The anomalous couplings $\mathrm{f_5^V}$ lead to violation of C and P symmetries while $\mathrm{f_4^V}$ introduces CP violation. At tree level these couplings are zero in the SM.

In order to calculate the impact of anomalous couplings on the measured distributions in the process $\mathrm{e^+e^-} \rightarrow \mathrm{f\bar{f}f'\bar{f}'}$, the EXCALIBUR generator is extended [20]. All matrix elements of conversion diagrams with two Z bosons, $\mathrm{M_{ZZ}}(\{\mathrm{p}^\nu\}, \lambda)$ are supplemented by an additional term containing anomalous couplings, $\mathrm{M_{AC}}(\{\mathrm{p}^\nu\}, \lambda, \mathrm{f_i^V})$ [19], where $\{\mathrm{p}^\nu\}$ represents the phase space variables and λ the helicities of initial and final state fermions.

Four–fermion Monte Carlo distributions for non-zero anomalous couplings are obtained by reweighting each event with the factor

$$\mathrm{W}(\{\mathrm{p}^\nu\}, \lambda, \mathrm{f_i^V}) \equiv \frac{\left|(\mathrm{M_{4f}}(\{\mathrm{p}^\nu\}, \lambda) + \mathrm{M_{AC}}(\{\mathrm{p}^\nu\}, \lambda, \mathrm{f_i^V}))\right|^2}{\left|\mathrm{M_{4f}}(\{\mathrm{p}^\nu\}, \lambda)\right|^2} \quad ,$$

where $\mathrm{M_{4f}}(\{\mathrm{p}^\nu\},\lambda)$ is the SM amplitude for the four–fermion final states, including in addition to $\mathrm{M_{ZZ}}(\{\mathrm{p}^\nu\},\lambda)$ also non–resonant diagrams. Initial state radiation is taken into account by evaluating the event weight at the centre–of–mass of the four–fermion system.

Using the distributions given in Figures 5 and 6, a binned maximum likelihood fit is performed for each of the anomalous couplings $\mathrm{f_i^V}$ fixing the others to zero. The results for all couplings are consistent with the SM values of zero and 95% confidence level limits on the parameters $\mathrm{f_i^V}$ are set

$$-3.6 \leq \mathrm{f_4^Z} \leq 3.4\ ,\ -8.4 \leq \mathrm{f_5^Z} \leq 7.9\ ,\ -2.1 \leq \mathrm{f_4^\gamma} \leq 2.1\ ,\ -4.9 \leq \mathrm{f_5^\gamma} \leq 4.8\ .$$

The couplings $\mathrm{f_i^\gamma}$ are independent from the couplings $\mathrm{h_i^Z}$ measured in $\mathrm{e^+e^-} \rightarrow \mathrm{Z}\gamma$ [21]. These are the first limits given for the couplings $\mathrm{f_i^V}$.

Acknowledgments

We wish to express our gratitude to the CERN accelerator divisions for the excellent performance and the successful upgrade of the LEP machine. We acknowledge the contributions of all the engineers and technicians who have participated in the construction and maintenance of this experiment.

References

[1] S.L. Glashow, Nucl. Phys. **22** (1961) 579;
S. Weinberg, Phys. Rev. Lett. **19** (1967) 1264;
A. Salam, “Elementary Particle Theory”, Ed. N. Svartholm, Stockholm, “Almquist and Wiksell” (1968), 367.

[2] “Physics at LEP2”, Eds. G. Altarelli, T. Sjöstrand and F. Zwirner, CERN 96-01 (1996).

[3] L3 Collaboration, M. Acciari *et al.*, Phys. Lett. **B 413** (1997) 191.

[4] L3 Collaboration, B. Adeva *et al.*, Nucl. Instr. Meth. **A 289** (1990) 35; M. Chemarin *et al.*, Nucl. Instr. Meth. **A 349** (1994) 345; M. Acciarri *et al.*, Nucl. Instr. Meth. **A 351** (1994) 300; G. Basti *et al.*, Nucl. Instr. Meth. **A 374** (1996) 293; I. C. Brock *et al.*, Nucl. Instr. Meth. **A 381** (1996) 236; A. Adam *et al.*, Nucl. Instr. Meth. **A 383** (1996) 342.

[5] F. A. Berends, R. Kleiss and R. Pittau, Nucl. Phys. **B 424** (1994) 308; Nucl. Phys. **B 426** (1994) 344; Nucl. Phys. (Proc. Suppl.) **B 37** (1994) 163; Phys. Lett. **B 335** (1994) 490; R. Kleiss and R. Pittau, Comp. Phys. Comm. **83** (1994) 14.

[6] T. Sjöstrand, CERN-TH/7112/93 (1993), revised August 1995; T. Sjöstrand, Comp. Phys. Comm. **82** (1994) 74; T. Sjöstrand, CERN-TH 7112/93 (1993, revised August 1994).

[7] S. Jadach, B. F. L. Ward and Z. Wąs, Comp. Phys. Comm. **79** (1994) 503.

[8] J. H. Field, Phys. Lett. **B 323** (1994) 432; J. H. Field and T. Riemann, Comp. Phys. Comm. **94** (1996) 53.

[9] M. Skrzypek *et al.*, Comp. Phys. Comm. **94** (1996) 216; M. Skrzypek *et al.*, Phys. Lett. **B 372** (1996) 289.

[10] R. Engel, Z. Phys. **C 66** (1995) 203; R. Engel and J. Ranft, Phys. Rev. **D 54** (1996) 4244.

[11] F. A. Berends, P. H. Daverfeldt and R. Kleiss, Nucl. Phys. **B 253** (1985) 441.

[12] R. Brun *et al.*, preprint CERN DD/EE/84-1 (Revised 1987).

[13] H. Fesefeldt, RWTH Aachen Report PITHA 85/02 (1985).

[14] The LEP Energy Working Group, “LEP energy calibration above the W pair production threshold”, LEP ECAL/98-02, ICHEP-98/352, July 1998.

[15] S. Bethke *et al.*, Nucl. Phys. **B 370** (1992) 310.

[16] S. Catani *et al.*, Phys. Lett. **B 263** (1991) 491.

[17] L. Lönnblad, C. Peterson and T. Rognvaldsson, Nucl. Phys. **B 349** (1991) 675.

[18] L3 Collaboration, M. Acciarri *et al.*, Phys. Lett. **B 431** (1998) 437.

[19] K. Hagiwara *et al.*, Nucl. Phys. **B 282** (1987) 253.

[20] J. Alcaraz *et al.*, CIEMAT-870 Report, December 1998.

[21] L3 Collaboration, M. Acciarri *et al.*, Phys. Lett. **B 436** (1998) 187.

The L3 Collaboration:

M.Acciarri,[26] P.Achard,[18] O.Adriani,[15] M.Aguilar-Benitez,[25] J.Alcaraz,[25] G.Alemanni,[21] J.Allaby,[16] A.Aloisio,[28] M.G.Alviggi,[28] G.Ambrosi,[18] H.Anderhub,[47] V.P.Andreev,[6,36] T.Angelescu,[12] F.Anselmo,[9] A.Arefiev,[27] T.Azemoon,[3] T.Aziz,[10] P.Bagnaia,[35] L.Baksay,[42] A.Balandras,[4] R.C.Ball,[3] S.Banerjee,[10] Sw.Banerjee,[10] K.Banicz,[44] A.Barczyk,[47,45] R.Barillère,[16] L.Barone,[35] P.Bartalini,[21] M.Basile,[9] R.Battiston,[32] A.Bay,[21] F.Becattini,[15] U.Becker,[14] F.Behner,[47] J.Berdugo,[25] P.Berges,[14] B.Bertucci,[32] B.L.Betev,[47] S.Bhattacharya,[10] M.Biasini,[32] A.Biland,[47] J.J.Blaising,[4] S.C.Blyth,[33] G.J.Bobbink,[2] A.Böhm,[1] L.Boldizsar,[13] B.Borgia,[16,35] D.Bourilkov,[47] M.Bourquin,[18] S.Braccini,[18] J.G.Branson,[38] V.Brigljevic,[47] F.Brochu,[4] A.Buffini,[15] A.Buijs,[43] J.D.Burger,[14] W.J.Burger,[32] J.Busenitz,[42] A.Button,[3] X.D.Cai,[14] M.Campanelli,[47] M.Capell,[14] G.Cara Romeo,[9] G.Carlino,[28] A.M.Cartacci,[15] J.Casaus,[25] G.Castellini,[15] F.Cavallari,[35] N.Cavallo,[28] C.Cecchi,[18] M.Cerrada,[25] F.Cesaroni,[22] M.Chamizo,[25] Y.H.Chang,[49] U.K.Chaturvedi,[17] M.Chemarin,[24] A.Chen,[49] G.Chen,[7] G.M.Chen,[7] H.F.Chen,[19] H.S.Chen,[7] X.Chereau,[4] G.Chiefari,[28] L.Cifarelli,[37] F.Cindolo,[9] C.Civinini,[15] I.Clare,[14] R.Clare,[14] G.Coignet,[4] A.P.Colijn,[2] N.Colino,[25] F.Conventi,[28] S.Costantini,[8] F.Cotorobai,[12] B.de la Cruz,[25] A.Csilling,[13] T.S.Dai,[14] J.A.van Dalen,[30] R.D'Alessandro,[15] R.de Asmundis,[28] P.Deglon,[18] A.Degré,[4] K.Deiters,[45] M.Della Pietra,[28] D.della Volpe,[28] P.Denes,[34] F.DeNotaristefani,[35] A.De Salvo,[47] M.Diemoz,[35] D.van Dierendonck,[2] F.Di Lodovico,[47] C.Dionisi,[16,35] M.Dittmar,[47] A.Dominguez,[38] A.Doria,[28] M.T.Dova,[17,♯] D.Duchesneau,[4] D.Dufournand,[4] P.Duinker,[2] I.Duran,[39] H.El Mamouni,[24] A.Engler,[33] F.J.Eppling,[14] F.C.Erné,[2] P.Extermann,[18] M.Fabre,[45] R.Faccini,[35] M.A.Falagan,[25] S.Falciano,[35] A.Favara,[15] J.Fay,[24] O.Fedin,[36] M.Felcini,[47] T.Ferguson,[33] F.Ferroni,[35] H.Fesefeldt,[1] E.Fiandrini,[32] J.H.Field,[18] F.Filthaut,[16] P.H.Fisher,[14] I.Fisk,[38] G.Forconi,[14] L.Fredj,[18] K.Freudenreich,[47] C.Furetta,[26] Yu.Galaktionov,[27,14] S.N.Ganguli,[10] P.Garcia-Abia,[5] M.Gataullin,[31] S.S.Gau,[11] S.Gentile,[35] N.Gheordanescu,[12] S.Giagu,[35] S.Goldfarb,[21] Z.F.Gong,[19] M.W.Gruenewald,[8] R.van Gulik,[2] V.K.Gupta,[34] A.Gurtu,[10] L.J.Gutay,[44] D.Haas,[5] A.Hasan,[29] D.Hatzifotiadou,[9] T.Hebbeker,[8] A.Hervé,[16] P.Hidas,[13] J.Hirschfelder,[33] H.Hofer,[47] G. Holzner,[47] H.Hoorani,[33] S.R.Hou,[49] I.Iashvili,[46] B.N.Jin,[7] L.W.Jones,[3] P.de Jong,[16] I.Josa-Mutuberría,[25] R.A.Khan,[17] D.Kamrad,[46] J.S.Kapustinsky,[23] M.Kaur,[17,◇] M.N.Kienzle-Focacci,[18] D.Kim,[35] D.H.Kim,[41] J.K.Kim,[41] S.C.Kim,[41] W.W.Kinnison,[23] J.Kirkby,[16] D.Kiss,[13] W.Kittel,[30] A.Klimentov,[14,27] A.C.König,[30] A.Kopp,[46] I.Korolko,[27] V.Koutsenko,[14,27] R.W.Kraemer,[33] W.Krenz,[1] A.Kunin,[14,27] P.Lacentre,[46,♮,♯] P.Ladron de Guevara,[25] I.Laktineh,[24] G.Landi,[15] C.Lapoint,[14] K.Lassila-Perini,[47] P.Laurikainen,[20] A.Lavorato,[37] M.Lebeau,[16] A.Lebedev,[14] P.Lebrun,[24] P.Lecomte,[47] P.Lecoq,[16] P.Le Coultre,[47] H.J.Lee,[8] J.M.Le Goff,[16] R.Leiste,[46] E.Leonardi,[35] P.Levtchenko,[36] C.Li,[19] C.H.Lin,[49] W.T.Lin,[49] F.L.Linde,[2,16] L.Lista,[28] Z.A.Liu,[7] W.Lohmann,[46] E.Longo,[35] Y.S.Lu,[7] K.Lübelsmeyer,[1] C.Luci,[16,35] D.Luckey,[14] L.Luminari,[35] W.Lustermann,[47] W.G.Ma,[19] M.Maity,[10] G.Majumder,[10] L.Malgeri,[16] A.Malinin,[27] C.Maña,[25] D.Mangeol,[30] P.Marchesini,[47] G.Marian,[42,¶] J.P.Martin,[24] F.Marzano,[35] G.G.G.Massaro,[2] K.Mazumdar,[10] R.R.McNeil,[6] S.Mele,[16] L.Merola,[28] M.Meschini,[15] W.J.Metzger,[30] M.von der Mey,[1] D.Migani,[9] A.Mihul,[12] H.Milcent,[16] G.Mirabelli,[35] J.Mnich,[16] P.Molnar,[8] B.Monteleoni,[15] T.Moulik,[10] G.S.Muanza,[24] F.Muheim,[18] A.J.M.Muijs,[2] S.Nahn,[14] M.Napolitano,[28] F.Nessi-Tedaldi,[47] H.Newman,[31] T.Niessen,[1] A.Nippe,[21] A.Nisati,[35] H.Nowak,[46] Y.D.Oh,[41] G.Organtini,[35] R.Ostonen,[20] C.Palomares,[25] D.Pandoulas,[1] S.Paoletti,[35,16] P.Paolucci,[28] H.K.Park,[33] I.H.Park,[41] G.Pascale,[35] G.Passaleva,[16] S.Patricelli,[28] T.Paul,[11] M.Pauluzzi,[32] C.Paus,[16] F.Pauss,[47] D.Peach,[16] M.Pedace,[35] Y.J.Pei,[1] S.Pensotti,[26] D.Perret-Gallix,[4] B.Petersen,[30] S.Petrak,[8] D.Piccolo,[28] M.Pieri,[15] P.A.Piroué,[34] E.Pistolesi,[26] V.Plyaskin,[27] M.Pohl,[47] V.Pojidaev,[27,15] H.Postema,[14] J.Pothier,[16] N.Produit,[18] D.Prokofiev,[36] J.Quartieri,[37] G.Rahal-Callot,[47] N.Raja,[10] P.G.Rancoita,[26] G.Raven,[38] P.Razis,[29] D.Ren,[47] M.Rescigno,[35] S.Reucroft,[11] T.van Rhee,[43] S.Riemann,[46] K.Riles,[3] A.Robohm,[47] J.Rodin,[42] B.P.Roe,[3] L.Romero,[25] S.Rosier-Lees,[4] J.A.Rubio,[16] D.Ruschmeier,[8] H.Rykaczewski,[47] S.Sakar,[35] J.Salicio,[16] E.Sanchez,[25] M.P.Sanders,[30] M.E.Sarakinos,[20] C.Schäfer,[1] V.Schegelsky,[36] S.Schmidt-Kaerst,[1] D.Schmitz,[1] N.Scholz,[47] H.Schopper,[48] D.J.Schotanus,[30] J.Schwenke,[1] G.Schwering,[1] C.Sciacca,[28] D.Sciarrino,[18] L.Servoli,[32] S.Shevchenko,[31] N.Shivarov,[40] V.Shoutko,[27] J.Shukla,[23] E.Shumilov,[27] A.Shvorob,[31] T.Siedenburg,[1] D.Son,[41] B.Smith,[33] P.Spillantini,[15] M.Steuer,[14] D.P.Stickland,[34] A.Stone,[6] H.Stone,[34] B.Stoyanov,[40] A.Straessner,[1] K.Sudhakar,[10] G.Sultanov,[17] L.Z.Sun,[19] H.Suter,[47] J.D.Swain,[17] Z.Szillasi,[42,¶] X.W.Tang,[7] L.Tauscher,[5] L.Taylor,[11] C.Timmermans,[30] Samuel C.C.Ting,[14] S.M.Ting,[14] S.C.Tonwar,[10] J.Tóth,[13] C.Tully,[34] K.L.Tung,[7] Y.Uchida,[14] J.Ulbricht,[47] E.Valente,[35] G.Vesztergombi,[13] I.Vetlitsky,[27] G.Viertel,[47] S.Villa,[11] M.Vivargent,[4] S.Vlachos,[5] H.Vogel,[33] H.Vogt,[46] I.Vorobiev,[16,27] A.A.Vorobyov,[36] A.Vorvolakos,[29] M.Wadhwa,[5] W.Wallraff,[1] J.C.Wang,[14] X.L.Wang,[19] Z.M.Wang,[19] A.Weber,[1] M.Weber,[1] P.Wienemann,[1] H.Wilkens,[30] S.X.Wu,[14] S.Wynhoff,[1] L.Xia,[31] Z.Z.Xu,[19] B.Z.Yang,[19] C.G.Yang,[7] H.J.Yang,[7] M.Yang,[7] J.B.Ye,[19] S.C.Yeh,[50] J.M.You,[33] An.Zalite,[36] Yu.Zalite,[36] P.Zemp,[47] Z.P.Zhang,[19] G.Y.Zhu,[7] R.Y.Zhu,[31] A.Zichichi,[9,16,17] F.Ziegler,[46] G.Zilizi,[42,¶] M.Zöller.[1]

1 I. Physikalisches Institut, RWTH, D-52056 Aachen, FRG[§]
III. Physikalisches Institut, RWTH, D-52056 Aachen, FRG[§]
2 National Institute for High Energy Physics, NIKHEF, and University of Amsterdam, NL-1009 DB Amsterdam, The Netherlands
3 University of Michigan, Ann Arbor, MI 48109, USA
4 Laboratoire d'Annecy-le-Vieux de Physique des Particules, LAPP,IN2P3-CNRS, BP 110, F-74941 Annecy-le-Vieux CEDEX, France
5 Institute of Physics, University of Basel, CH-4056 Basel, Switzerland
6 Louisiana State University, Baton Rouge, LA 70803, USA
7 Institute of High Energy Physics, IHEP, 100039 Beijing, China[△]
8 Humboldt University, D-10099 Berlin, FRG[§]
9 University of Bologna and INFN-Sezione di Bologna, I-40126 Bologna, Italy
10 Tata Institute of Fundamental Research, Bombay 400 005, India
11 Northeastern University, Boston, MA 02115, USA
12 Institute of Atomic Physics and University of Bucharest, R-76900 Bucharest, Romania
13 Central Research Institute for Physics of the Hungarian Academy of Sciences, H-1525 Budapest 114, Hungary[‡]
14 Massachusetts Institute of Technology, Cambridge, MA 02139, USA
15 INFN Sezione di Firenze and University of Florence, I-50125 Florence, Italy
16 European Laboratory for Particle Physics, CERN, CH-1211 Geneva 23, Switzerland
17 World Laboratory, FBLJA Project, CH-1211 Geneva 23, Switzerland
18 University of Geneva, CH-1211 Geneva 4, Switzerland
19 Chinese University of Science and Technology, USTC, Hefei, Anhui 230 029, China[△]
20 SEFT, Research Institute for High Energy Physics, P.O. Box 9, SF-00014 Helsinki, Finland
21 University of Lausanne, CH-1015 Lausanne, Switzerland
22 INFN-Sezione di Lecce and Universitá Degli Studi di Lecce, I-73100 Lecce, Italy
23 Los Alamos National Laboratory, Los Alamos, NM 87544, USA
24 Institut de Physique Nucléaire de Lyon, IN2P3-CNRS,Université Claude Bernard, F-69622 Villeurbanne, France
25 Centro de Investigaciones Energéticas, Medioambientales y Tecnologícas, CIEMAT, E-28040 Madrid, Spain[♭]
26 INFN-Sezione di Milano, I-20133 Milan, Italy
27 Institute of Theoretical and Experimental Physics, ITEP, Moscow, Russia
28 INFN-Sezione di Napoli and University of Naples, I-80125 Naples, Italy
29 Department of Natural Sciences, University of Cyprus, Nicosia, Cyprus
30 University of Nijmegen and NIKHEF, NL-6525 ED Nijmegen, The Netherlands
31 California Institute of Technology, Pasadena, CA 91125, USA
32 INFN-Sezione di Perugia and Universitá Degli Studi di Perugia, I-06100 Perugia, Italy
33 Carnegie Mellon University, Pittsburgh, PA 15213, USA
34 Princeton University, Princeton, NJ 08544, USA
35 INFN-Sezione di Roma and University of Rome, "La Sapienza", I-00185 Rome, Italy
36 Nuclear Physics Institute, St. Petersburg, Russia
37 University and INFN, Salerno, I-84100 Salerno, Italy
38 University of California, San Diego, CA 92093, USA
39 Dept. de Fisica de Particulas Elementales, Univ. de Santiago, E-15706 Santiago de Compostela, Spain
40 Bulgarian Academy of Sciences, Central Lab. of Mechatronics and Instrumentation, BU-1113 Sofia, Bulgaria
41 Center for High Energy Physics, Adv. Inst. of Sciences and Technology, 305-701 Taejon, Republic of Korea
42 University of Alabama, Tuscaloosa, AL 35486, USA
43 Utrecht University and NIKHEF, NL-3584 CB Utrecht, The Netherlands
44 Purdue University, West Lafayette, IN 47907, USA
45 Paul Scherrer Institut, PSI, CH-5232 Villigen, Switzerland
46 DESY-Institut für Hochenergiephysik, D-15738 Zeuthen, FRG
47 Eidgenössische Technische Hochschule, ETH Zürich, CH-8093 Zürich, Switzerland
48 University of Hamburg, D-22761 Hamburg, FRG
49 National Central University, Chung-Li, Taiwan, China
50 Department of Physics, National Tsing Hua University, Taiwan, China

§ Supported by the German Bundesministerium für Bildung, Wissenschaft, Forschung und Technologie
‡ Supported by the Hungarian OTKA fund under contract numbers T019181, F023259 and T024011.
¶ Also supported by the Hungarian OTKA fund under contract numbers T22238 and T026178.
♭ Supported also by the Comisión Interministerial de Ciencia y Tecnología.
♯ Also supported by CONICET and Universidad Nacional de La Plata, CC 67, 1900 La Plata, Argentina.
♮ Supported by Deutscher Akademischer Austauschdienst.
◇ Also supported by Panjab University, Chandigarh-160014, India.
△ Supported by the National Natural Science Foundation of China.

$\ell^+\ell^-\mathrm{q\bar{q}}$ final states	σ(pb)	$\ell^+\ell^-\ell'^+\ell'^-$ final states	σ(pb)	$\ell^+\ell^-\ell'^+\ell'^-$ final states	σ(pb)
$\mathrm{e^+e^-q\bar{q}}$	1.42	$\mathrm{e^+e^-e^+e^-}$	0.31	$\mu^+\mu^-\mu^+\mu^-$	0.006
$\mu^+\mu^-\mathrm{q\bar{q}}$	0.18	$\mathrm{e^+e^-}\mu^+\mu^-$	0.33	$\mu^+\mu^-\tau^+\tau^-$	0.013
$\tau^+\tau^-\mathrm{q\bar{q}}$	0.18	$\mathrm{e^+e^-}\tau^+\tau^-$	0.33	$\tau^+\tau^-\tau^+\tau^-$	0.006

Table 1: Cross sections calculated with EXCALIBUR for the four–fermion processes at 182.72 GeV centre-of-mass energy using the signal definition given in the text.

$\ell^+\ell^-\mathrm{q\bar{q}}$ selection		
Process	Expected Events	Signal efficiency (%)
$\mathrm{e^+e^-q\bar{q}}$	6.1 ± 0.3	7.7
$\mu^+\mu^-\mathrm{q\bar{q}}$	1.60 ± 0.06	16.0
$\ell^+\ell^-\mathrm{q\bar{q}}$	7.7 ± 0.3	7.8
$\ell^+\ell^-\ell^+\ell^-$	0.12 ± 0.02	0.2
$\ell^+\ell^-\mathrm{q\bar{q}} + \ell^+\ell^-\ell^+\ell^-$	7.8 ± 0.3	
Background	1.6 ± 0.1	
Total Events	9.5 ± 0.3	
Data	12	
$\ell^+\ell^-\ell'^+\ell'^-$ selection		
Process	Expected Events	Signal Efficiency (%)
$\mathrm{e^+e^-e^+e^-}$	2.65 ± 0.03	15.3
$\mathrm{e^+e^-}\mu^+\mu^-$	1.61 ± 0.04	8.9
$\mathrm{e^+e^-}\tau^+\tau^-$	0.48 ± 0.02	2.7
$\mu^+\mu^-\mu^+\mu^-$	0.093 ± 0.003	26.4
$\mu^+\mu^-\tau^+\tau^-$	0.103 ± 0.004	14.3
$\tau^+\tau^-\tau^+\tau^-$	0.023 ± 0.001	6.4
$\ell^+\ell^-\ell^+\ell^-$	4.96 ± 0.05	9.1
$\ell^+\ell^-\mathrm{q\bar{q}}$	0.10 ± 0.03	0.1
$\ell^+\ell^-\ell^+\ell^- + \ell^+\ell^-\mathrm{q\bar{q}}$	5.06 ± 0.06	
Background	5.4 ± 1.1	
Total Events	10.5 ± 1.1	
Data	12	

Table 2: Number of expected four–fermion and background events and number of observed data events after the $\ell^+\ell^-\mathrm{q\bar{q}}$ and $\ell^+\ell^-\ell'^+\ell'^-$ selections. The signal efficiencies are also reported.

ZZ →	σ(fb)	ZZ →	σ(fb)	ZZ →	σ(fb)	ZZ →	σ(fb)
$\mathrm{u\bar{u}u\bar{u}}$	4.89	$\mathrm{u\bar{u}d\bar{d}}$	8.39	$\mathrm{u\bar{u}c\bar{c}}$	6.88		
$\mathrm{u\bar{u}s\bar{s}}$	8.50	$\mathrm{d\bar{d}d\bar{d}}$	5.60	$\mathrm{d\bar{d}s\bar{s}}$	10.5	$\sum \mathrm{q\bar{q}q'\bar{q}'}$	116
$\mathrm{u\bar{u}}\nu_\mathrm{e}\bar{\nu}_\mathrm{e}$	3.35	$\mathrm{u\bar{u}}\nu_\mu\bar{\nu}_\mu$	3.85	$\mathrm{d\bar{d}}\nu_\mathrm{e}\bar{\nu}_\mathrm{e}$	4.10		
$\mathrm{d\bar{d}}\nu_\mu\bar{\nu}_\mu$	4.76					$\sum \mathrm{q\bar{q}}\nu\bar{\nu}$	63.0
$\mathrm{u\bar{u}e^+e^-}$	3.31	$\mathrm{u\bar{u}}\mu^+\mu^-$	2.21	$\mathrm{d\bar{d}e^+e^-}$	3.86		
$\mathrm{d\bar{d}}\mu^+\mu^-$	2.73					$\sum \ell^+\ell^-\mathrm{q\bar{q}}$	43.4
$\mathrm{e^+e^-}\nu_\mathrm{e}\bar{\nu}_\mathrm{e}$	1.49	$\mathrm{e^+e^-}\nu_\mu\bar{\nu}_\mu$	1.73	$\mu^+\mu^-\nu_\mathrm{e}\bar{\nu}_\mathrm{e}$	1.09		
$\mu^+\mu^-\nu_\mu\bar{\nu}_\mu$	1.19	$\mu^+\mu^-\nu_\tau\bar{\nu}_\tau$	1.24			$\sum \ell^+\ell^-\nu\bar{\nu}$	12.0
$\mathrm{e^+e^-e^+e^-}$	1.43	$\mathrm{e^+e^-}\mu^+\mu^-$	1.30	$\mu^+\mu^-\mu^+\mu^-$	0.88		
$\mu^+\mu^-\tau^+\tau^-$	0.71					$\sum \ell^+\ell^-\ell'^+\ell'^-$	6.50
$\nu_\mathrm{e}\bar{\nu}_\mathrm{e}\nu_\mathrm{e}\bar{\nu}_\mathrm{e}$	0.78	$\nu_\mathrm{e}\bar{\nu}_\mathrm{e}\nu_\mu\bar{\nu}_\mu$	1.87	$\nu_\mu\bar{\nu}_\mu\nu_\mu\bar{\nu}_\mu$	1.04		
$\nu_\mu\bar{\nu}_\mu\nu_\tau\bar{\nu}_\tau$	2.16					$\sum \nu\bar{\nu}\nu'\bar{\nu}'$	8.76
						$\sum \mathrm{f\bar{f}f'\bar{f}'}$	250

Table 3: Cross sections calculated with EXCALIBUR for the ZZ signal at centre–of–mass energy of 182.72 GeV.

Process ZZ →	Signal (%) efficiency	Signal events	Background events	Data events
$\mathrm{e^+e^-q\bar{q}}$	79	0.79 ± 0.03	0.29 ± 0.04	2
$\mu^+\mu^-\mathrm{q\bar{q}}$	58	0.42 ± 0.02	0.09 ± 0.01	0
$\tau^+\tau^-\mathrm{q\bar{q}}$	36	0.26 ± 0.01	0.85 ± 0.13	0
$\ell^+\ell^-\ell'^+\ell'^-$	15–78	0.13 ± 0.01	0.12 ± 0.03	0
$\ell^+\ell^-\nu\bar{\nu}$	33–37	0.18 ± 0.02	1.23 ± 0.12	2
$\mathrm{q\bar{q}}\nu\bar{\nu}$	47	1.64 ± 0.07	13.0 ± 0.7	12
$\mathrm{q\bar{q}q'\bar{q}'}$	34	2.26 ± 0.14	46 ± 2	47

Table 4: Signal efficiencies, expected number of signal and background events and data for all ZZ final states investigated.

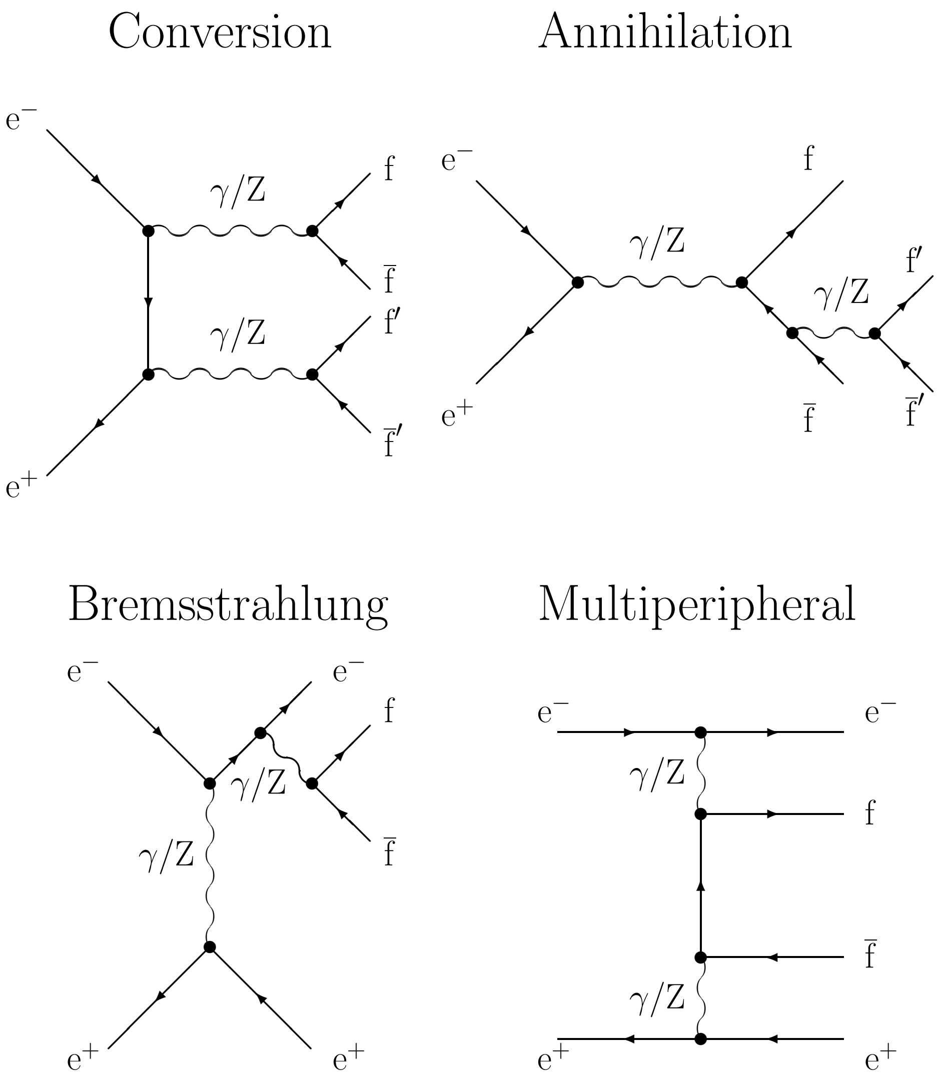

Figure 1: Lowest order Feynman diagrams for the neutral–current $e^+e^- \to f\bar{f}f'\bar{f}'$ processes.

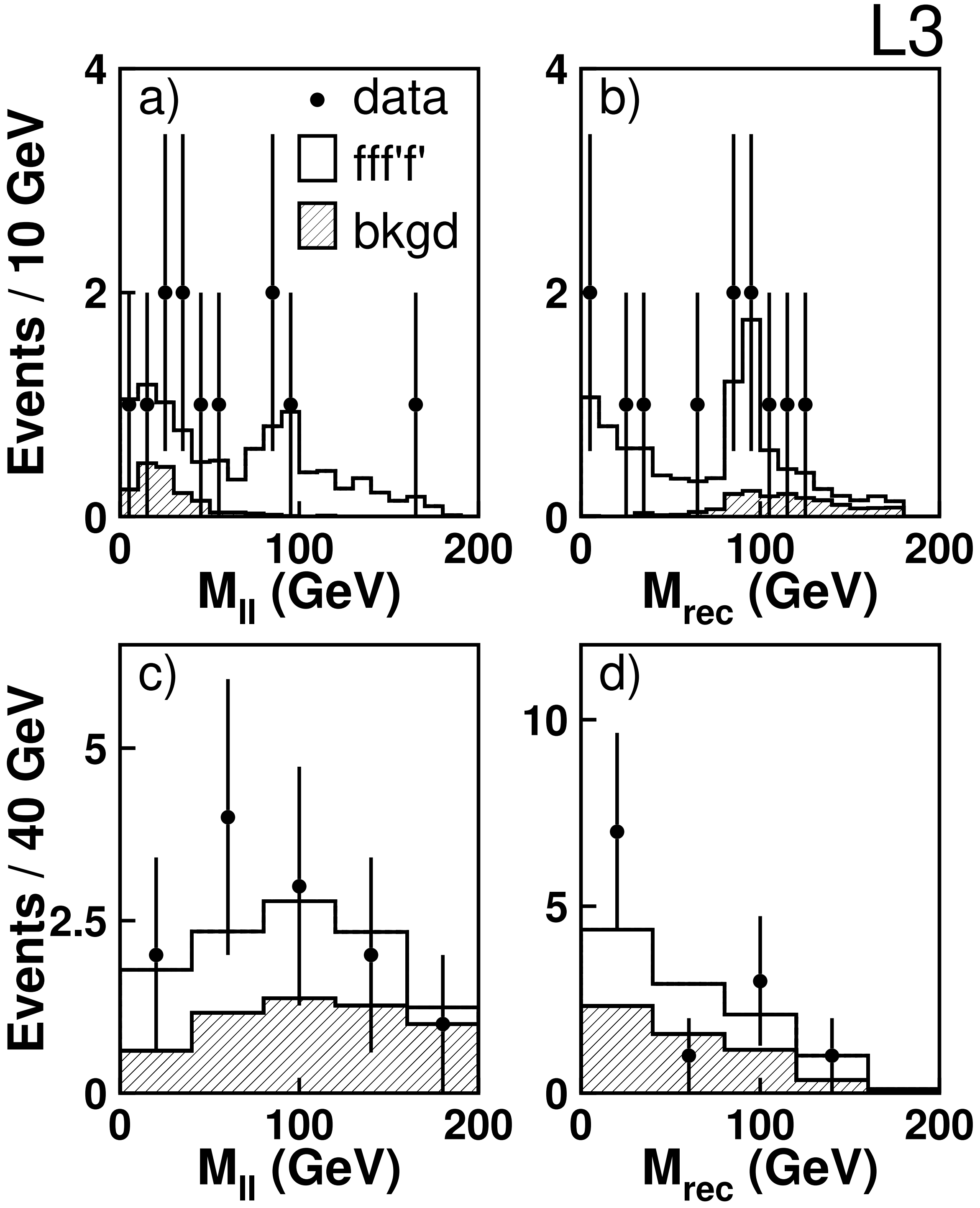

Figure 2: The invariant mass of the electron and muon pairs (a) and their recoil mass (b) after the $\ell^+\ell^-\mathrm{q\bar{q}}$ selection; the highest invariant mass of the pair of leptons of the same flavour (c) and their recoil mass (d) after the $\ell^+\ell^-\ell'^+\ell'^-$ selection.

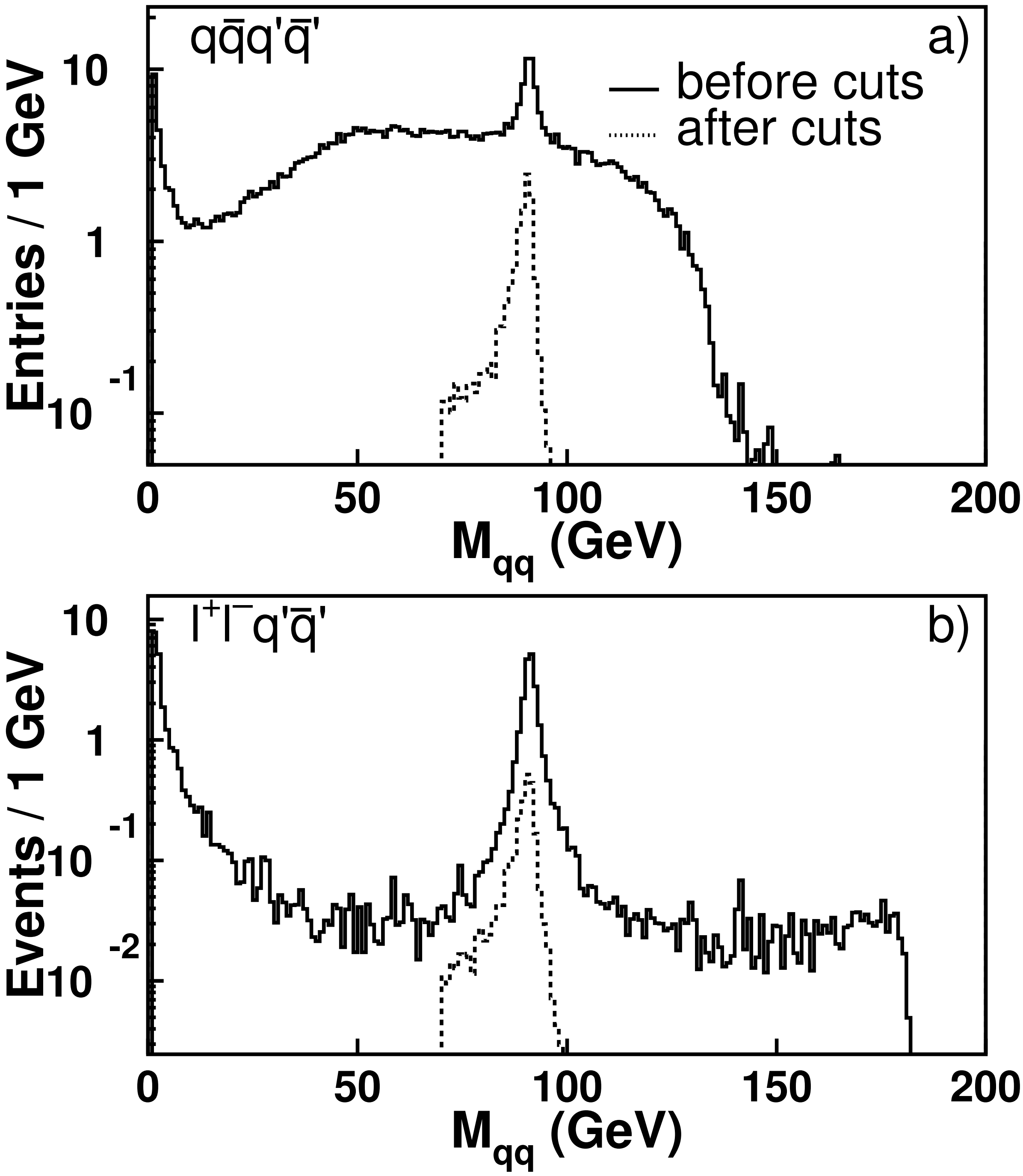

Figure 3: The EXCALIBUR generated distributions of the quark pair mass before (full line) and after (dashed line) generator cuts, as described in the text, for the (a) $e^+e^- \to q\bar{q}q'\bar{q}'$ and the (b) $e^+e^- \to \ell^+\ell^- q\bar{q}$ events at $\sqrt{s}$= 182.72 GeV. The number of events is normalised to 55.3 pb^{-1} of luminosity.

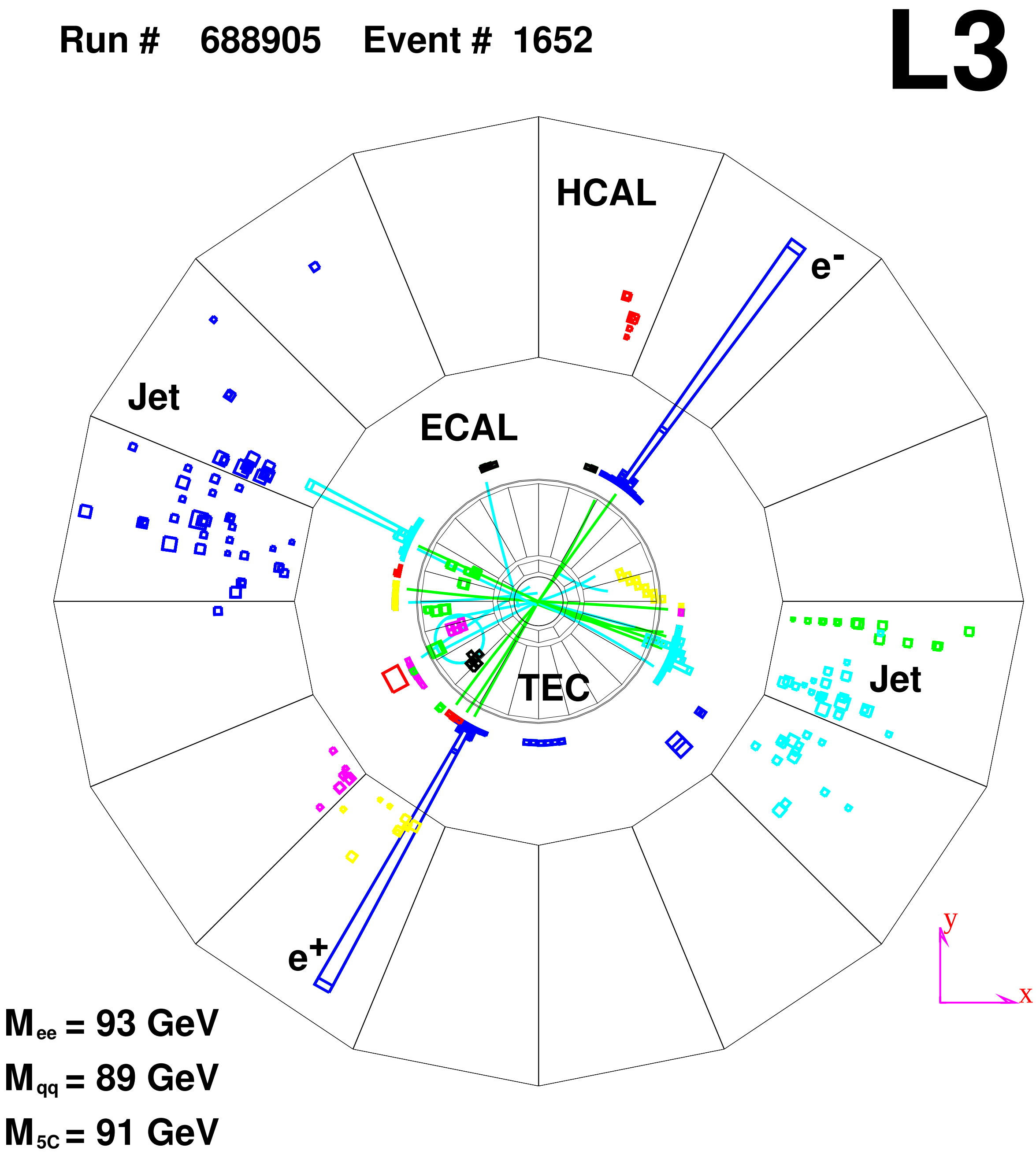

Figure 4: Event selected by the $e^+e^- \to ZZ \to \ell^+\ell^- q\bar{q}$ selection. Displayed are the tracks in the central tracking chamber (TEC) and the energy depositions in the electromagnetic (ECAL) and hadronic (HCAL) calorimeters. Two electrons and two jets are present in the event. M_{ee} and M_{qq} are the electron pair and the jet pair masses after kinematic fit imposing total four–momentum conservation. M_{5C} is the mass resulting from the kinematic fit imposing in addition equal electron pair and jet pair masses.

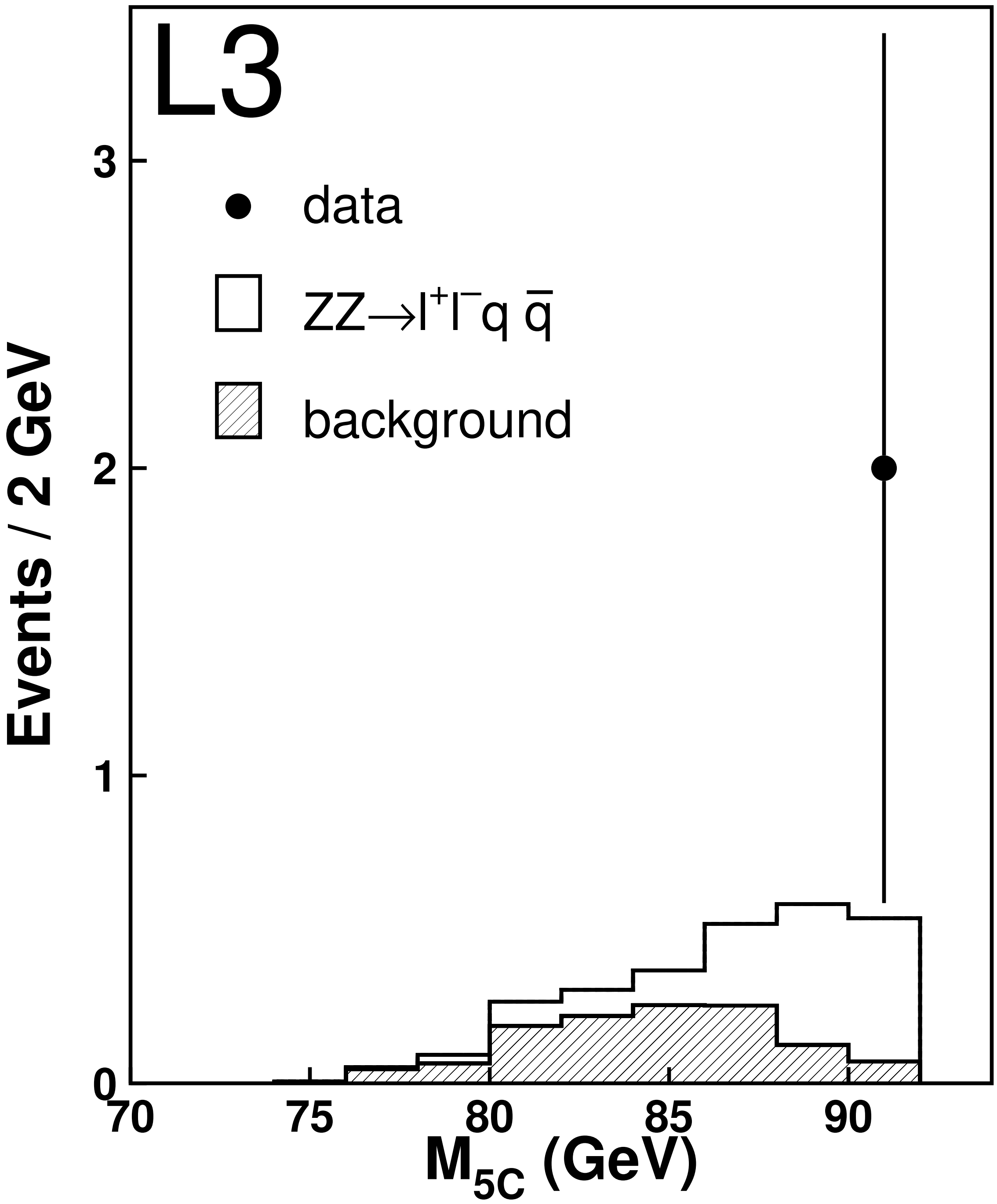

Figure 5: Distribution of M_{5C}, the mass obtained from a kinematic fit imposing four–momentum conservation and equal masses of the lepton pair and the jet pair, after the $\ell^+\ell^-q\bar{q}$ selections.

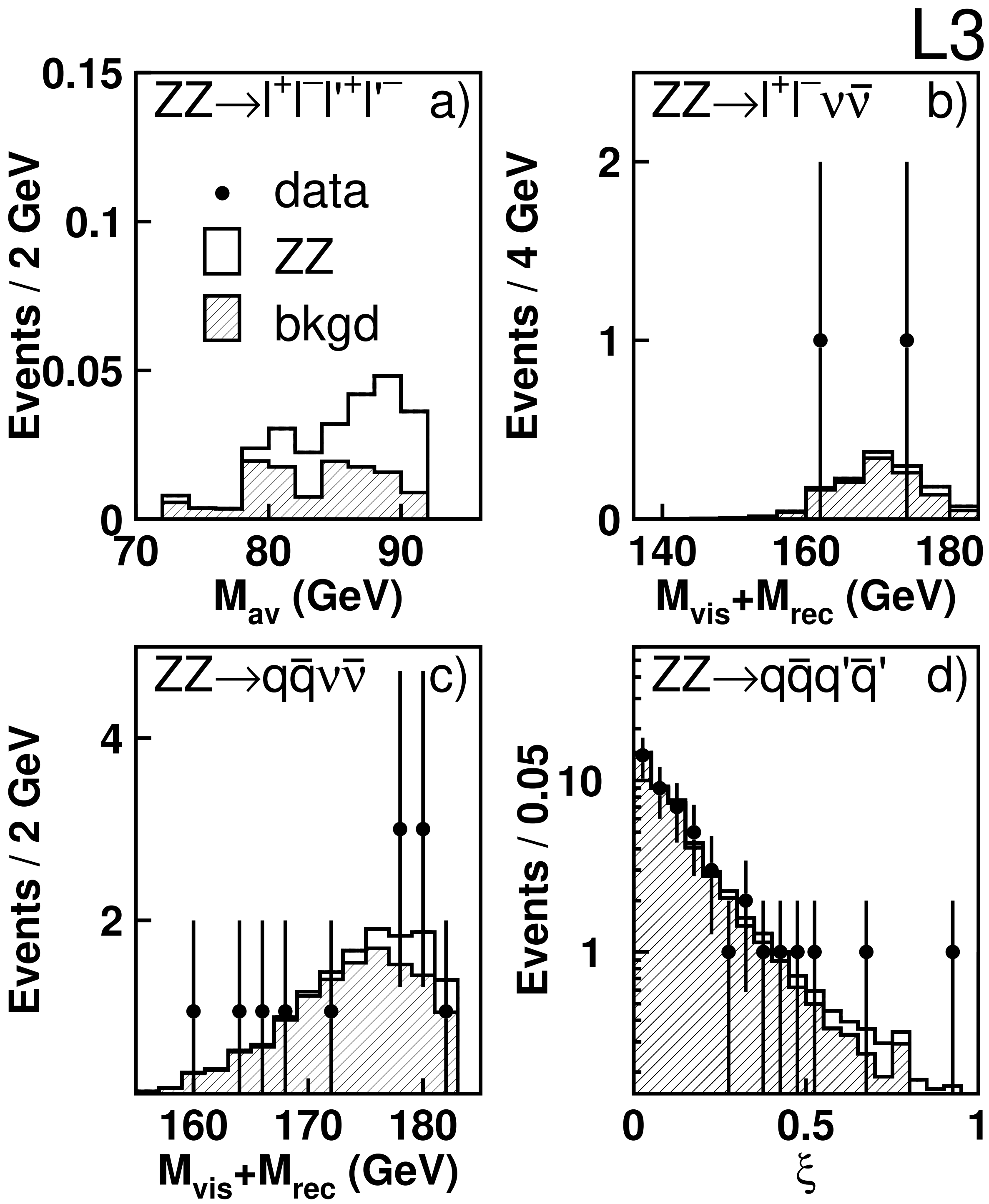

Figure 6: (a) The average of the lepton pair mass closest to the Z boson mass and its recoil mass, M_{av}, after the $\ell^+\ell^-\ell'^+\ell'^-$ selection, (b) the sum of the visible mass and the recoil mass after the $\ell^+\ell^-\nu\bar{\nu}$ and (c) the $q\bar{q}\nu\bar{\nu}$ selections and (d) the ξ variable (see text) after the $q\bar{q}q'\bar{q}'$ selection.

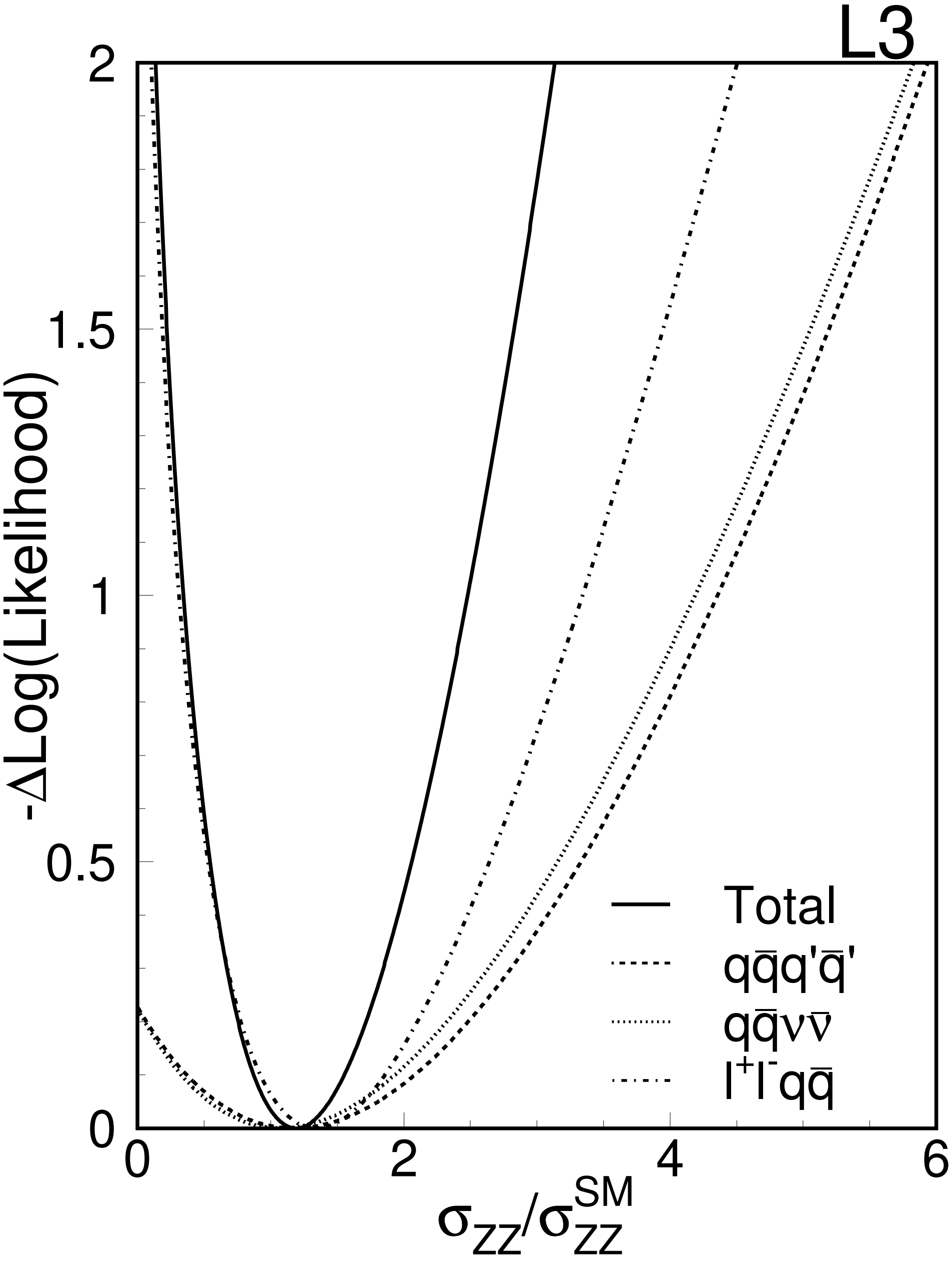

Figure 7: Separate and combined likelihoods as a function of the ratio between the measured ZZ cross section, σ_{ZZ}, and the value predicted by the SM, $\sigma_{\mathrm{ZZ}}^{\mathrm{SM}}$.